C. R. Mecanique 344 (2016) 569–581

Contents lists available at ScienceDirect

Comptes Rendus Mecanique

www.sciencedirect.com

# Wave propagation in a strongly heterogeneous elastic porous medium: Homogenization of Biot medium with double porosities

## *Propagation d'ondes dans un milieu élastique poreux fortement hétérogène : homogénéisation d'un milieu de Biot avec porosités doubles*

Eduard Rohan [a], Salah Naili [b,*], Vu-Hieu Nguyen [b]

[a] *European Centre of Excellence, NTIS – New Technologies for Information Society Faculty of Applied Sciences, University of West Bohemia, Univerzitnií 22, 30614 Pilsen, Czech Republic*

[b] *Université Paris-Est, Laboratoire "Modélisation et simulation multi-échelle", MSME UMR 8208 CNRS, 61, avenue du Général-de-Gaulle, 94010 Créteil cedex, France*

ARTICLE INFO

*Article history:*
Received 20 January 2016
Accepted 2 May 2016
Available online 1 June 2016

*Keywords:*
Poroelasticity
Asymptotic homogenization
Double-porosity
Wave propagation
Effective properties

*Mots-clés :*
Poroélasticité
Homogénéisation asymptotique
Double porosité
Propagation d'ondes
Propriétés effectives

ABSTRACT

We study wave propagation in an elastic porous medium saturated with a compressible Newtonian fluid. The porous network is interconnected whereby the pores are characterized by two very different characteristic sizes. At the mesoscopic scale, the medium is described using the Biot model, characterized by a high contrast in the hydraulic permeability and anisotropic elasticity, whereas the contrast in the Biot coupling coefficient is only moderate. Fluid motion is governed by the Darcy flow model extended by inertia terms and by the mass conservation equation. The homogenization method based on the asymptotic analysis is used to obtain a macroscopic model. To respect the high contrast in the material properties, they are scaled by the small parameter, which is involved in the asymptotic analysis and characterized by the size of the heterogeneities. Using the estimates of wavelengths in the double-porosity networks, it is shown that the macroscopic descriptions depend on the contrast in the static permeability associated with pores and micropores and on the frequency. Moreover, the microflow in the double porosity is responsible for fading memory effects via the macroscopic poroviscoelastic constitutive law.



RÉSUMÉ

Nous étudions la propagation des ondes dans un milieu poreux élastique dont le réseau poreux est interconnecté et saturé par un fluide newtonien compressible. On suppose que la taille caractéristique des micropores est très hétérogène dans le réseau poreux. Le milieu est caractérisé par un contraste élevé de perméabilités et d'élasticités anisotropes et par un contraste modéré pour le coefficient de couplage de Biot. À l'échelle mésoscopique, le mouvement du fluide est régi par le modèle d'écoulement de Darcy étendu avec des termes d'inertie et par l'équation de conservation de la masse. Le matrice poreuse est décrite en

* Corresponding author.
*E-mail addresses:* rohan@kme.zcu.cz (E. Rohan), salah.naili@univ-paris-est.fr (S. Naili), vu-hieu.nguyen@univ-paris-est.fr (V.-H. Nguyen).

http://dx.doi.org/10.1016/j.crme.2016.05.001

utilisant le modèle de Biot. La méthode d'homogénéisation *via* l'analyse asymptotique à double échelle est utilisée pour obtenir un modèle macroscopique pour des contrastes élevés de perméabilité et d'élasticité anisotrope, mais avec des contrastes modérés du coefficient de couplage de Biot, lesquels ont été mis à l'échelle par rapport à la taille des hétérogénéités. À partir de l'estimation des longueurs d'onde dans les deux réseaux, il est montré que, non seulement la description macroscopique dépend du contraste de perméabilité statique entre les pores et micropores et de la fréquence, mais aussi que la double porosité est responsable des effets de mémoire *via* la loi de comportement poroviscoélastique.



## 1. Introduction

Wave propagation belongs to one of the most challenging issues in modelling fluid-saturated elastic porous media. Although the topic has been studied over the past decades and several modelling approaches and particular models have been proposed, the dispersion phenomenon has not yet been fully understood. This study is motivated by the need to understand the behavior of strongly heterogeneous media subjected to incident waves. Besides the natural materials, such as soils, rocks, wood, or bones, the potential applications of the theory reported below are in the field of metamaterials, *i.e.* artificial materials engineered to have properties that may not be found in nature. The design and manufacturing of such materials has become possible thanks to the progress made in both materials science and mechanical engineering. They are constituted by conventional materials, such as metals, or plastics arranged to form special periodic patterns at the microscopic level. Metamaterials gain their properties due to their exactly-designed structures. Their precise shape, geometry, size, orientation and arrangement can affect wave propagation in an unconventional manner, creating material properties that are unachievable with conventional materials.

In a general setting, fluid-saturated porous (poroelastic) media are constituted by a solid (elastic) skeleton in which the fluid-saturated pores are distributed as a connected pore network, or as densely distributed particles. When a unique microscopic characteristic size can be defined according to the pore size, such a medium can be studied with a "single" porosity type model. However, many natural, as well as artificial porous materials exhibit the presence of heterogeneity at scales much larger than microstructure ones, but much smaller than the wavelengths. In such a porous medium with heterogeneity at the mesoscopic scale, pore fluids in regions of dissimilar properties respond differently to changes in their fluid pressures. In principle, for simulating the wave propagation in such mesoscopic heterogeneous media, a continuum porous model with spatially varying coefficients may be used. For media with periodically distributed inhomogeneities at the meso-scale, macroscopic effective media can be derived from the continuum equations established at mesoscopic scale. In this paper, we consider a "double"-porosity type of poroelastic media, which consists of two linear anisotropic porous constituents, whereby their porous systems are interconnected.

The notion of the double porosity is usually associated with other material structures, such as fractured porous rocks, which (at the mesoscopic scale) consist of a fluid interacting with a skeleton which itself is a microporous medium. Many authors have studied these fluid-saturated porous (poroelastic) media with double porosity by using the various methods, among which the phenomenological approach (see for instance [1,2]) and the homogenization approach (see for instance [3,4]) can be distinguished. As an advantage, the latter one provides more rigorous a way for obtaining the equations at the macroscopic scale, governing the response of the fluid-saturated elastic media with a double porosity, but also allows us to define the effective properties at the macroscopic scale using the material properties and the geometrical features at the microscopic (or mesoscopic) scale. In this framework, some authors have focused on the acoustic response of such porous media (see, for instance, [5–9]).

However, the present work deals with another characterization of a "double-porosity" (or double permeability) medium as a periodic mixture of two different porous media that occupy two disjoint subdomains at the mesoscopic scale. The domain $\Omega$ is occupied by a periodic mixture consisting of two disjoint elastic porous materials (components) situated in domains $\Omega_c$ and $\Omega_m$, following the notations introduced in Rohan [10]. The behaviours of the two components are governed by the Biot–Darcy model. The decomposition in the two subdomains $\Omega_c$ and $\Omega_m$ generates the spatial heterogeneity of permeability, which will be in the focus of our study (see Fig. 1). In particular, we consider "high permeability contrast" media featured by large differences in the intrinsic permeability magnitudes between the two components. In addition to the contrast in the permeability, we consider also a high contrast in the anisotropic elasticity and in the Biot coupling coefficients. Apart of artificial metamaterial structures, which are in our focus, a similar arrangement can also be found in some vegetable concretes. Within the context of sustainable development and noise reduction, "vegetable concrete," which is comprised of renewable material (vegetables particles or fibres as hemp, wood, rubberwood) and different binders (cement or lime), appears to be an interesting solution.

Macroscopic material (effective) properties of the upscaled medium are linked to the properties of the phases that constitute the structure at the mesoscopic scale; they are determined by the geometry of the microstructure and the mechanical

properties of its microscopic constituents. Understanding the interplay between the combination of these hierarchically arranged ingredients is necessary for the prediction of the effective material behavior and, in the context of metamaterial design, for the optimization of the microstructure to enhance the material's performances. With the help of bottom-up manufacturing techniques, a large number of micrometer-scale designs can now be reduced to the nanometer scale and, therefore, can bring completely new quality. The tools needed to create metamaterials include modelling, geometry and property design, bottom-up manufacturing and structural characterization at the nanoscale. By controlling the positioning of nano-inclusions, nanostructured metamaterials can been designed for interesting fields of applications where wave propagation is involved.

For the comprehension of the macroscopic behavior of these materials, the homogenization method developed from 1980s [11–13] presents a very useful and efficient modelling tool that establishes rigorous links between the multiple scales relevant for the whole hierarchical structure. The homogenization method used for upscaling the thermodynamic systems described by boundary value problems involving partial differential equations and boundary conditions is based on the asymptotic analysis with respect to the scale parameter. To study rigorously such systems by means of functional analysis, the two-scale convergence [14] or the periodic unfolding method of homogenization [15] can be used. As an advantage, the results, *i.e.* formulations of the local cell problems, the "global" homogenized models, and expressions for computing the homogenized coefficients, are given in forms that can be transformed easily by finite element discretization to obtain numerical results.

## 2. Description of the heterogeneous poroelastic medium

In what follows, the equations are formulated in a Cartesian framework of reference $\mathcal{R}(\mathrm{O};\boldsymbol{e}_1,\boldsymbol{e}_2,\boldsymbol{e}_3)$, where $O$ is the origin of the space and $(\boldsymbol{e}_1,\boldsymbol{e}_2,\boldsymbol{e}_3)$ is an orthonormal basis for this space. The coordinates of a point $M$ are specified by $x=(x_1,x_2,x_3)$ in $\mathcal{R}$. We denote the angular frequency by $\omega$. The gradient and divergence operators are respectively denoted by $\nabla$ and $\nabla\cdot$. When these operators have a subscript which is space variable, it is for indicating that the operator acts relatively to this space variable, for instance $\nabla_x=(\partial_i^x)$. The dot symbol '$\cdot$' denotes the scalar product between two vectors and the colon symbol ':' stands for the scalar (inner) product of two second-order tensors.

By $\partial\Omega$ we designate the boundary of domain $\Omega$. The following functional spaces are used: by $L^2(\Omega)$ we refer to square integrable functions defined in domain $\Omega$; by $H^1(\Omega)$ we mean the Sobolev space $W^{1,2}(\Omega)\subset L^2(\Omega)$ formed by square integrable functions including their first generalized derivatives; space $H^1_0(\Omega)\subset H^1(\Omega)$ is constituted by functions with zero trace on $\partial\Omega$; the bold notation is used to denote spaces of vector-valued functions, e.g., $\mathbf{H}^1(\Omega)$; by subscript $_\#$ we refer to the *Y-periodic functions*; by $\mathbf{H}_0(\mathrm{div},\Omega)$ we denote vectorial functions from $\mathbf{L}^2(\Omega)$ with divergence in $L^2(\Omega)$ and vanishing projection on the normal at $\partial\Omega$ (see, *e.g.*, [16]).

### 2.1. Mesoscopic model

The models of the fluid-saturated porous (poroelastic) media that we have in mind are relevant to the scale where individual fluid-filled pores are not distinguishable so that, at any point of the bulk material, both solid and fluid phases are present according to the volume fractions. We shall call such a scale the "physically mesoscopic scale". In particular, we consider the following system of partial differential equations proposed by Biot [17,18] and revised by Auriault et al. [19]

$$\begin{aligned}
-\nabla\cdot(\mathbb{D}\boldsymbol{e}(\boldsymbol{u}))+\nabla\cdot(\boldsymbol{\alpha}p)-\omega^2\bar{\rho}\boldsymbol{u}+\mathrm{i}\omega\rho^{\mathrm{f}}\boldsymbol{w}&=0\\
-\omega^2\rho^{\mathrm{f}}\boldsymbol{u}+\eta[\boldsymbol{k}(\omega)]^{-1}\boldsymbol{w}+\nabla p&=0\\
\mathrm{i}\omega\boldsymbol{\alpha}:\boldsymbol{e}(\boldsymbol{u})+\nabla\cdot\boldsymbol{w}+\frac{\mathrm{i}\omega}{\mu}p&=0
\end{aligned}\tag{1}$$

consisting of the momentum equation $(1)_1$, the generalized extended Darcy law $(1)_2$, and the fluid volume conservation $(1)_3$. For the sake of simplicity, we omit the volume forces. In equations (1), the vector $\boldsymbol{u}$ is the displacement field describing the solid skeleton kinematics, the second-order tensor $\boldsymbol{e}(\boldsymbol{u})$ is the small strain tensor, the scalar $p$ is the fluid pressure, the vector $\boldsymbol{w}=\phi_0(\boldsymbol{v}^{\mathrm{f}}-\boldsymbol{v}^{\mathrm{s}})$ describes the Darcian relative fluid velocity with respect to the solid skeleton involving the velocity vector field of fluid $\boldsymbol{v}^{\mathrm{f}}$ and solid skeleton $\boldsymbol{v}^{\mathrm{s}}$, and the reference volume fraction of the fluid $\phi_0$. By $\rho^{\mathrm{s}}$ and $\rho^{\mathrm{f}}$ we denote the intrinsic density of the solid phase and fluid density at rest, respectively; hence $\bar{\rho}=\rho^{\mathrm{s}}(1-\phi_0)+\phi_0\rho^{\mathrm{f}}$ is the mean density. The material properties are defined by the elasticity fourth-order tensor $\mathbb{D}$ of the drained solid skeleton, by the Biot bulk modulus $\mu$ of the solid–fluid mixture, by the second-order tensor of the Biot effective stress coefficient $\boldsymbol{\alpha}$, and by the second-order tensor $\boldsymbol{k}(\omega)$ of dynamic permeability, which is a frequency-dependent complex-valued second-order tensor. Note that the dependence of $\boldsymbol{k}$ on the frequency enables us to study the response of the system for arbitrary frequency (*i.e.* the high- and low-frequency behaviours). This tensor contains the inertial drag and viscous dissipative effects due to the pore motion fluid [20]. This splitting up is introduced in what follows.

All the material parameters listed above are defined for a given porous solid skeleton defined at the "physically mesoscopic scale". Of course, there is a smaller "physically microscopic scale", where fluid and solid regions are clearly separate, but the parts occupied either by the fluid or by the solid are geometrically distinguishable. In this context, the mesoscopic model (1) can be considered as a result of a "homogenization" of a dynamic fluid–structure interaction problem.

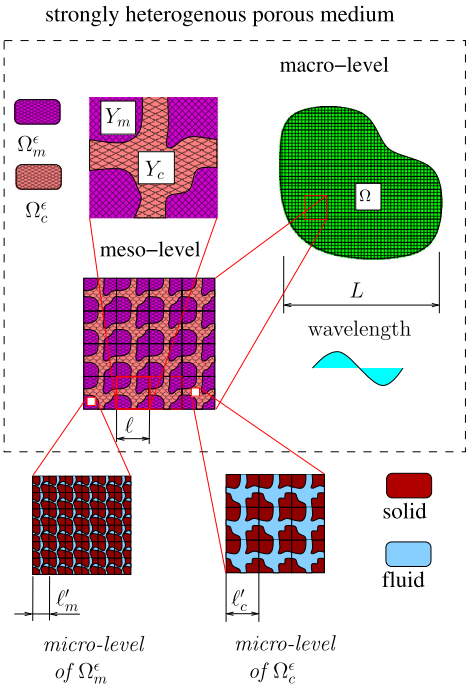


**Fig. 1.** Schematic illustration of a periodic elastic porous medium: mesoporosities formed by fluid and solid parts lead to large contrasts in the permeability and the material properties; the characteristic lengths are defined from $L$ at the macroscopic scale, $\ell$ at the mesoscopic scale, and $\ell'_{c,m}$ at the microscopic scale.

To formulate a boundary value problem with equations (1) prescribed in an open bounded domain $\Omega \subset \mathbb{R}^3$, we shall consider the following boundary conditions on $\partial\Omega$:

$$\boldsymbol{u} = \bar{\boldsymbol{u}}\,, \quad \boldsymbol{w}\cdot\boldsymbol{n} = 0 \tag{2}$$

where $\bar{\boldsymbol{u}}$ is sufficiently regular and $\boldsymbol{n}$ is the unit outward normal on $\partial\Omega$.

In Auriault et al. [19] and Nguyen et al. [21], it has been shown that $\eta[\boldsymbol{k}(\omega)]^{-1}$ can be defined from its inverse by the relation:

$$\eta[\boldsymbol{k}(\omega)]^{-1} = [\boldsymbol{\kappa}(\omega)]^{-1} = \left(\mathrm{i}\omega\boldsymbol{\rho} + [\boldsymbol{K}]^{-1}\right) \tag{3}$$

where $\boldsymbol{\rho}$ and $\boldsymbol{K}$ are real-valued, second-order tensors associated with the inertia and viscous effects, respectively. Note that the second-order tensor $\boldsymbol{\rho}$ (in bold) linked to inertia effects must not to be confused with the mean density $\bar{\rho}$. If $\boldsymbol{K}$ is a given constant, the inertia effects are well approximated in model (1) for low frequencies, or slow transition events. Should also the higher frequencies be respected, $\boldsymbol{K}$ would depend on the particular frequency of incident waves considered. In Nguyen et al. [21] such a situation has been explored for a rigid skeleton.

### 2.2. Periodic structure with double porosity

The heterogeneous elastic porous medium occupying domain $\Omega$ consists of two distinct parts with different magnitudes of the hydraulic permeability. A dimensionless scale parameter $\varepsilon$ is introduced as the ratio between the characteristic size of the heterogeneity at the mesoscopic scale (characteristic length $\ell$) and the wavelength which is comparable with a macroscopic size $L$, thus, $\varepsilon = \ell/L$ (see Fig. 1). For a fixed $\varepsilon > 0$ we consider the decomposition of an open bounded domain $\Omega \subset \mathbb{R}^3$ into two parts, a matrix $\Omega^\varepsilon_{\mathrm{m}}$ and channels $\Omega^\varepsilon_{\mathrm{c}}$. More precisely, with $\Omega = \Omega^\varepsilon_{\mathrm{m}} \cup \Omega^\varepsilon_{\mathrm{c}} \cup \Gamma^\varepsilon$ with $\Omega^\varepsilon_{\mathrm{m}} \cap \Omega^\varepsilon_{\mathrm{c}} = \emptyset$, where $\Gamma^\varepsilon = \overline{\Omega}^\varepsilon_{\mathrm{m}} \cap \overline{\Omega}^\varepsilon_{\mathrm{c}}$ is the interface. We require that $\Omega^\varepsilon_{\mathrm{c}}$ is connected and its boundary $\partial\Omega^\varepsilon_{\mathrm{c}}$ is Lipschitz. In what follows, labelling by one of two subscripts (or superscripts), m and c referring to different material subdomains, the *matrix* and the *channels*, respectively, is employed.

By virtue of the periodically distributed heterogeneity, $\Omega$ is generated as a periodic lattice using the representative elementary volume (REV) occupying elementary cell $Y$ defined by $Y = \prod_{i=k}^{3} ]0, \ell_k[$. For any given $\varepsilon > 0$ we define coordinates $y = (y_k) \in Y$ which are given for $k = 1, 2, 3$ by: $y_k = (x_k - \ell_k[x_k/\ell_k]_Y)/\varepsilon$ where $[x_k/\ell_k]_Y$ denotes the integer part of $x_k/\ell_k$. At the mesoscopic scale, the heterogeneous structure is a periodic lattice generated by the representative cell $Y$ which is decomposed into two disjoint parts $Y_{\mathrm{c}}$ and $Y_{\mathrm{m}}$ corresponding to the two micropores distributed periodically in subdomains $\Omega^\varepsilon_{\mathrm{c}}$ and $\Omega^\varepsilon_{\mathrm{m}}$, respectively (see Fig. 1), thus, $Y_{\mathrm{c}} = Y \setminus \overline{Y}_{\mathrm{m}}$.

The reason for such a domain decomposition is related to assumed discontinuities in material coefficients on interface $\Gamma^\varepsilon$; in general, we may consider piecewise-continuous material coefficients which are introduced, as follows:

$$\begin{aligned}
\bar\rho^\varepsilon &= \chi_{\rm m}(y)\bar\rho_{\rm m}(y) + \chi_{\rm c}(y)\bar\rho_{\rm c}(y)\\
\boldsymbol{\rho}^\varepsilon &= \chi_{\rm m}(y)\boldsymbol{\rho}_{\rm m}(y) + \chi_{\rm c}(y)\boldsymbol{\rho}_{\rm c}(y)\\
\mu^\varepsilon &= \chi_{\rm m}(y)\mu_{\rm m}(y) + \chi_{\rm c}(y)\mu_{\rm c}(y)\\
\mathbb{D}^\varepsilon &= \chi_{\rm m}(y)\mathbb{D}_{\rm m}(y) + \varepsilon^2\chi_{\rm c}(y)\widehat{\mathbb{D}}_{\rm c}(y)\\
\boldsymbol{\alpha}^\varepsilon &= \chi_{\rm m}(y)\boldsymbol{\alpha}_{\rm m}(y) + \varepsilon\chi_{\rm c}(y)\boldsymbol{\alpha}_{\rm c}(y)\\
\boldsymbol{K}^\varepsilon &= \varepsilon^2\chi_{\rm m}(y)\widehat{\boldsymbol{K}}_{\rm m}(y) + \chi_{\rm c}(y)\boldsymbol{K}_{\rm c}(y)
\end{aligned} \tag{4}$$

where $\chi_d$ for $d = {\rm m}, {\rm c}$ are the characteristic functions of domains $Y_d$.

The motivation for the above decomposition corresponds to a situation, where the channels contain fluid and a very porous, well permeable skeleton; this can be made of a network of thin entangled fibres. Therefore, the elasticity $\mathbb{D}^\varepsilon$ is scaled by $\varepsilon^2$ in the domain $\Omega_{\rm c}^\varepsilon$, to capture the compliance. In the matrix, $\Omega_{\rm m}^\varepsilon$, the medium is formed by a much stiffer skeleton, however, the permeability $\boldsymbol{K}^\varepsilon$ is much smaller than that in the channels, therefore the scaling $\varepsilon^2$ is adopted according to Rohan [10]. The scaling of the Biot coupling coefficients $\boldsymbol{\alpha}^\varepsilon$ by $\varepsilon$ in $\Omega_{\rm c}^\varepsilon$, while $\mu^\varepsilon$ is independent of $\varepsilon$, is necessary to obtain a nontrivial limit behaviour, as the consequence of scaling the elasticity coefficients.

The double-porosity type scaling was proposed by Arbogast et al. [22] and used also in our recent related works [10,21,23]. It is combined here with the analogous-type scaling of the elasticity in the complementary part of the mesoscopic structure. It is worth noting that the same scaling ansatz was employed to study wave dispersion in the strongly heterogeneous periodic elastic solids [24–26]. Obviously, the scaling ansatz proposed above is not the only possible and physically motivated definition. Smyshlyaev [27] considered elastic solids where $\mathbb{D}^\varepsilon = \chi_{\rm m}(y)\mathbb{D}_{\rm m}(y) + \chi_{\rm c}(y)(\varepsilon^2\widehat{\mathbb{D}}_{\rm c}(y) + \overline{\mathbb{D}}_{\rm c}(y))$, where $\overline{\mathbb{D}}_{\rm c}$ is a positive semi-definite tensor. Using such an ansatz, one can describe different behaviours of the elastic material in $Y_{\rm c}$ with respect to the bulk and deviatoric parts of the strain. We shall pursue such a treatment in a future work.

## 3. Main result – homogenized model

The upscaling procedure of the heterogeneous continuum consists of the limit analysis of the solution to the weak formulation (5) with respect to $\varepsilon \to 0$. For this, we use the periodic unfolding method [28,23] based on the coordinate decomposition $x = \xi + \varepsilon y$, where $\xi = \varepsilon\left[\frac{x}{\varepsilon}\right]_Y$ is the lattice coordinate at the mesoscopic scale, thus given by the brackets, so that $y \in Y$ is the local coordinate of the microscopic scale.

*Weak formulation* We consider the weak formulation of the problem described by the system (1) with the boundary conditions (2). Since the coefficients introduced in (4) are discontinuous on interfaces $\Omega_{\rm m}^\varepsilon \cap \Omega_{\rm c}^\varepsilon$, the differential equations (1) must be supplemented by transmission conditions on these interface; besides the continuity of the pressure field $p$ and the displacement field $\boldsymbol{u}$, also the normal flux of the fluid $\boldsymbol{w}\cdot\boldsymbol{n}$ and the interface traction $\mathbf{T} = \boldsymbol{\sigma}\boldsymbol{n}$ are assumed, where $\boldsymbol{\sigma} = \mathbb{D}\boldsymbol{e}(\boldsymbol{u}) - \boldsymbol{\alpha}\, p$ is the effective stress relevant to the mesoscopic scale.

The quantities involved in the boundary value problem are labelled with superscript $^\varepsilon$ to respect their dependence on the scale parameter.

Find $(\boldsymbol{u}^\varepsilon, \boldsymbol{w}^\varepsilon, p^\varepsilon) \in \mathbf{H}^1_{\tilde{\boldsymbol{u}}}(\Omega)\times\mathbf{L}^2(\Omega)\times L^2(\Omega)$, which satisfy

$$\begin{aligned}
-\omega^2\int_\Omega \bar\rho^\varepsilon\boldsymbol{u}^\varepsilon\cdot\tilde{\boldsymbol{v}} + {\rm i}\omega\int_\Omega \rho^{\rm f}\boldsymbol{w}^\varepsilon\cdot\tilde{\boldsymbol{v}} + \int_\Omega [\mathbb{D}^\varepsilon\boldsymbol{e}(\boldsymbol{u}^\varepsilon)] : \boldsymbol{e}(\tilde{\boldsymbol{v}}) - \int_\Omega p^\varepsilon\,\boldsymbol{\alpha}^\varepsilon : \boldsymbol{e}(\tilde{\boldsymbol{v}}) = 0\\
{\rm i}\omega\int_\Omega \boldsymbol{\rho}^\varepsilon\boldsymbol{w}^\varepsilon\cdot\tilde{\boldsymbol{w}} - \omega^2\int_\Omega \rho^{\rm f}\boldsymbol{u}^\varepsilon\cdot\tilde{\boldsymbol{w}} + \int_\Omega [\boldsymbol{K}^\varepsilon]^{-1}\boldsymbol{w}^\varepsilon\cdot\tilde{\boldsymbol{w}} + \int_\Omega \nabla p^\varepsilon\cdot\tilde{\boldsymbol{w}} = 0\\
{\rm i}\omega\int_\Omega \tilde q\,\boldsymbol{\alpha}^\varepsilon : \boldsymbol{e}(\boldsymbol{u}^\varepsilon) + \int_\Omega \tilde q\nabla\cdot\boldsymbol{w}^\varepsilon + {\rm i}\omega\int_\Omega \frac{1}{\mu^\varepsilon}p^\varepsilon\tilde q = 0
\end{aligned} \tag{5}$$

for all $(\tilde{\boldsymbol{v}}, \tilde{\boldsymbol{w}}, \tilde p) \in \mathbf{H}^1_0(\Omega)\times\mathbf{L}^2(\Omega)\times L^2(\Omega)$. The set $\mathbf{H}^1_{\tilde{\boldsymbol{u}}}(\Omega) \subset \mathbf{H}^1(\Omega)$ is formed by functions satisfying the boundary condition $(2)_1$.

### 3.1. Two-scale limit problem

Using estimates on the solution to Eq. (5) the convergence result can be established, which yields the following recovery sequences defined in terms of functions $\mathbf{Q}^{{\rm R}\varepsilon} = (\boldsymbol{u}^{0,{\rm R}\varepsilon}, \hat{\boldsymbol{u}}^{{\rm R}\varepsilon}, \boldsymbol{U}^{1,{\rm R}\varepsilon}, \boldsymbol{W}^{{\rm R}\varepsilon}, \hat{\boldsymbol{w}}^{{\rm R}\varepsilon}, p^{0,{\rm R}\varepsilon}, P^{1,{\rm R}\varepsilon}, \hat p^{{\rm R}\varepsilon})$

$$\begin{aligned}
\boldsymbol{u}^{\varepsilon}(x) &\sim \boldsymbol{u}^{0,\mathrm{R}\varepsilon}(x) + \chi_{\mathrm{c}}(y)\hat{\boldsymbol{u}}^{\mathrm{R}\varepsilon}(x,y) + \chi_{\mathrm{m}}(y)\varepsilon \boldsymbol{U}^{1,\mathrm{R}\varepsilon}(x,y)\\
\boldsymbol{w}^{\varepsilon}(x) &\sim \chi_{\mathrm{c}}(y)\boldsymbol{W}^{\mathrm{R}\varepsilon}(x,y) + \chi_{\mathrm{m}}(y)\varepsilon \hat{\boldsymbol{w}}^{\mathrm{R}\varepsilon}(x,y)\\
p^{\varepsilon}(x) &\sim p^{0,\mathrm{R}\varepsilon}(x) + \chi_{\mathrm{c}}(y)\varepsilon P^{1,\mathrm{R}\varepsilon}(x,y) + \chi_{\mathrm{m}}(y)\hat{p}^{\mathrm{R}\varepsilon}(x,y)
\end{aligned} \tag{6}$$

where $y = \frac{x}{\varepsilon} - \left[\frac{x}{\varepsilon}\right]_Y$.

We show that the functions $\mathbf{Q}^{\mathrm{R}\varepsilon}$ converge weakly to $\mathbf{Q} = (\boldsymbol{u}^0, \hat{\boldsymbol{u}}, \boldsymbol{U}^1, \boldsymbol{W}, \hat{\boldsymbol{w}}, p^0, P^1, \hat{p})$ in the unfolded space $L^2(\Omega \times Y)$, whereby all these limit functions $\mathbf{Q}(x,y)$ are $Y$-periodic in $y$. Moreover, $\boldsymbol{W} = 0$ in $Y_{\mathrm{m}}$ and, as will be shown below, $\nabla_y \cdot \boldsymbol{W} = 0$ in $Y_{\mathrm{c}}$, $\boldsymbol{W}\cdot\boldsymbol{n} = 0$ on $\partial Y_{\mathrm{c}} \cap \partial Y_{\mathrm{m}}$. The boundary condition $(2)_2$ holds for the mean seepage velocity, i.e. $\boldsymbol{w}^0 \cdot \boldsymbol{n} = 0$ on $\partial\Omega$, where $\boldsymbol{w}^0(x) = \int_Y \boldsymbol{W}(x,y)$. It should be noted that $\boldsymbol{u}^0(x)$ and $p^0(x)$ are the only macroscopic variables. The displacements satisfy $\boldsymbol{u}^0(x) = \bar{\boldsymbol{u}}$ on $\partial\Omega$. Further we shall use an abstract setting: by $\mathcal{A}$ we denote the *set of admissible two-scale solutions*, whereas the space $\tilde{\mathcal{A}}_0$ contains all the admissible test functions $\tilde{\mathbf{Q}}_0$ associated with $\mathbf{Q}$.

Upon substituting the recovery sequences in the unfolded (instead of the unfolding method of homogenization, the classical two-scale convergence can be used) form of problem (5), and using the corresponding recovery sequences of the type (6) adopted for the test functions $\tilde{\mathbf{Q}}_0 = (\boldsymbol{v}^0, \hat{\boldsymbol{v}}, \boldsymbol{V}^1, \boldsymbol{\psi}, \hat{\boldsymbol{\psi}}, q^0, Q^1, \hat{q}) \in \tilde{\mathcal{A}}_0$, the following two-scale limit problem imposed in $\Omega \times Y$ is obtained:

Find $\mathbf{Q} = (\boldsymbol{u}^0, \hat{\boldsymbol{u}}, \boldsymbol{U}^1, \boldsymbol{W}, \hat{\boldsymbol{w}}, p^0, P^1, \hat{p}) \in \mathcal{A}$ satisfying

$$\begin{aligned}
&-\omega^2 \int_\Omega \int_Y \bar{\rho}(\boldsymbol{u}^0 + \chi_{\mathrm{c}}\hat{\boldsymbol{u}})\cdot(\boldsymbol{v}^0 + \chi_{\mathrm{c}}\hat{\boldsymbol{v}}) + \mathrm{i}\omega \int_\Omega \int_{Y_{\mathrm{c}}} \rho^{\mathrm{f}} \boldsymbol{W}\cdot(\boldsymbol{v}^0 + \chi_{\mathrm{c}}\hat{\boldsymbol{v}})\\
&+ \int_\Omega \int_{Y_{\mathrm{c}}} \widehat{\mathbb{D}}_{\mathrm{c}} \boldsymbol{e}_y(\hat{\boldsymbol{u}}) : \boldsymbol{e}_y(\hat{\boldsymbol{v}}) + \int_\Omega \int_{Y_{\mathrm{m}}} \mathbb{D}_{\mathrm{m}}(\boldsymbol{e}_x(\boldsymbol{u}^0) + \boldsymbol{e}_y(\boldsymbol{U}^1)) : (\boldsymbol{e}_x(\boldsymbol{v}^0) + \boldsymbol{e}_y(\boldsymbol{V}^1))\\
&+ \int_\Omega \int_{Y_{\mathrm{c}}} \widehat{\boldsymbol{\alpha}}^c : \boldsymbol{e}_y(\hat{\boldsymbol{v}}) p^0 + \int_\Omega \int_{Y_{\mathrm{m}}} \boldsymbol{\alpha}^m : (\boldsymbol{e}_x(\boldsymbol{v}^0) + \boldsymbol{e}_y(\boldsymbol{V}^1))(p^0 + \hat{p}) = 0
\end{aligned} \tag{7}$$

for all $(\boldsymbol{v}^0, \boldsymbol{V}^1, \hat{\boldsymbol{v}}) \in \tilde{\mathcal{A}}_0$ (we adopt the inclusion $\tilde{\mathbf{Q}}_0 \in \tilde{\mathcal{A}}_0$ for the subset of relevant test functions), then

$$\begin{aligned}
&-\omega^2 \int_\Omega \int_Y \rho^{\mathrm{f}}(\boldsymbol{u}^0 + \chi_{\mathrm{c}}\hat{\boldsymbol{u}})\cdot\boldsymbol{\psi} + \mathrm{i}\omega \int_\Omega \int_{Y_{\mathrm{c}}} \boldsymbol{\rho}\boldsymbol{W}\cdot\boldsymbol{\psi} + \int_\Omega \int_{Y_{\mathrm{c}}} [\boldsymbol{K}_{\mathrm{c}}]^{-1}\boldsymbol{W}\cdot\boldsymbol{\psi}\\
&+ \int_\Omega \int_{Y_{\mathrm{m}}} [\widehat{\boldsymbol{K}}_{\mathrm{m}}]^{-1}\hat{\boldsymbol{w}}\cdot\hat{\boldsymbol{\psi}} + \int_\Omega \int_{Y_{\mathrm{c}}} (\nabla_x p^0 + \nabla_y P^1)\cdot\boldsymbol{\psi} + \int_\Omega \int_{Y_{\mathrm{m}}} \nabla_y \hat{p}\cdot\hat{\boldsymbol{\psi}} = 0
\end{aligned} \tag{8}$$

for all $(\boldsymbol{\psi}, \hat{\boldsymbol{\psi}}) \in \tilde{\mathcal{A}}_0$, and

$$\begin{aligned}
&\mathrm{i}\omega \int_\Omega \int_{Y_{\mathrm{c}}} \widehat{\boldsymbol{\alpha}}^c : \boldsymbol{e}_y(\hat{\boldsymbol{u}}) q^0 + \mathrm{i}\omega \int_\Omega \int_{Y_{\mathrm{m}}} \boldsymbol{\alpha}^m : (\boldsymbol{e}_x(\boldsymbol{u}^0) + \boldsymbol{e}_y(\boldsymbol{U}^1))(q^0 + \hat{q})\\
&- \int_\Omega \int_{Y_{\mathrm{c}}} (\nabla_x q^0 + \nabla_y Q^1)\cdot\boldsymbol{W} - \int_\Omega \int_{Y_{\mathrm{m}}} \nabla_y \hat{q}\cdot\hat{\boldsymbol{w}}\\
&+ \mathrm{i}\omega \int_\Omega \int_Y \frac{1}{\mu}\left(p^0 + \chi_{\mathrm{m}}\hat{p}\right)\left(q^0 + \chi_{\mathrm{m}}\hat{q}\right) = 0
\end{aligned} \tag{9}$$

for all $(q^0, Q^1, \hat{q}) \in \tilde{\mathcal{A}}_0$.

### 3.2. Macroscopic model

Using the classical procedure of the scale separation which is reported briefly in Section 4, the macroscopic equations of the homogenized model are obtained. The weak formulation of the macroscopic problem reads as follows.

Find $\boldsymbol{u}^0 \in \mathbf{H}^1_0(\Omega)$ and $p^0 \in H^1_0(\Omega)$ such that

$$\begin{aligned} -\omega^2 \int_\Omega \boldsymbol{\mathcal{M}}\boldsymbol{u}^0 \cdot \boldsymbol{v}^0 + \int_\Omega \left(\mathrm{i}\omega \boldsymbol{\mathcal{D}}\boldsymbol{e}(\boldsymbol{u}^0) - p^0 \boldsymbol{\mathcal{B}}\right) : \boldsymbol{e}(\boldsymbol{v}^0) \\ + \mathrm{i}\omega \int_\Omega \left(\mathrm{i}\omega \boldsymbol{\mathcal{G}} \nabla p^0 + \underline{\mathcal{C}} p^0\right) \cdot \boldsymbol{v}^0 = 0 \\ \int_\Omega \mathrm{i}\omega q^0 \boldsymbol{\mathcal{B}}' : \boldsymbol{e}(\boldsymbol{u}^0) - \omega^2 \int_\Omega \boldsymbol{u}^0 \cdot \left((\boldsymbol{\mathcal{G}}')^{\mathrm{T}} \nabla q^0 + \underline{\mathcal{C}}' q^0\right) \\ + \int_\Omega (\mathcal{K} \nabla p^0) \cdot \nabla q^0 + \mathrm{i}\omega \int_\Omega \mathcal{H} p^0 q^0 = 0 \end{aligned} \tag{10}$$

for all $\boldsymbol{v}^0 \in \mathbf{H}^1_0(\Omega)$ and $q^0 \in H^1_0(\Omega)$.

The homogenized coefficients $\boldsymbol{\mathcal{M}}, \boldsymbol{\mathcal{D}}, \boldsymbol{\mathcal{B}}, \boldsymbol{\mathcal{B}}', \boldsymbol{\mathcal{G}}, \boldsymbol{\mathcal{G}}', \underline{\mathcal{C}}, \underline{\mathcal{C}}', \mathcal{K}$ and $\mathcal{H}$ depend on the heterogeneity associated with the mesoscopic structure where material properties are defined according to (4). The following symmetries hold:

$$\begin{aligned} &\mathcal{D}_{ijkl} = \mathcal{D}_{klij} = \mathcal{D}_{jikl}\,, && \mathcal{B}_{ij} = \mathcal{B}'_{ij} = \mathcal{B}_{ji} \\ &\mathcal{G}'_{ji} = -\mathrm{i}\omega \mathcal{G}_{ij}\,, && \mathcal{C}'_i = -\mathcal{C}_i \\ &\mathcal{K}_{ij} = \mathcal{K}_{ji}\,, && \mathcal{M}_{ij} = \mathcal{M}_{ji} \end{aligned} \tag{11}$$

with an intrinsic notation, we have

$$\begin{aligned} &\boldsymbol{\mathcal{B}} = \boldsymbol{\mathcal{B}}' = \boldsymbol{\mathcal{B}}^{\mathrm{T}}\,, && \boldsymbol{\mathcal{G}}' = -\mathrm{i}\omega \boldsymbol{\mathcal{G}}^{\mathrm{T}} \\ &\underline{\mathcal{C}}' = -\underline{\mathcal{C}}\,, && \mathcal{K} = \mathcal{K}^{\mathrm{T}} \\ &\boldsymbol{\mathcal{M}} = \boldsymbol{\mathcal{M}}^{\mathrm{T}}\,, \end{aligned} \tag{12}$$

The differential form of the model can be retrieved from (10); assuming *periodic media* where all homogenized coefficients are constant in space (note that the same weak formulation can be obtained for a "slowly varying" heterogeneous medium, where the homogenized coefficients depend on $x$, see [29]), the macroscopic model is formed by the following equations where the above listed symmetries (11) are respected:

$$\begin{aligned} -\omega^2 \boldsymbol{\mathcal{M}}\boldsymbol{u}^0 - \nabla \cdot \left(\mathrm{i}\omega \boldsymbol{\mathcal{D}}\boldsymbol{e}(\boldsymbol{u}^0) - (\boldsymbol{\mathcal{B}} - \omega^2 \boldsymbol{\mathcal{G}}) p^0\right) + \mathrm{i}\omega \underline{\mathcal{C}} p^0 = 0 \quad &\text{in } \Omega \\ \mathrm{i}\omega \left(\boldsymbol{\mathcal{B}} - \omega^2 (\boldsymbol{\mathcal{G}})^{\mathrm{T}}\right) : \nabla \boldsymbol{u}^0 + \omega^2 \underline{\mathcal{C}} \cdot \boldsymbol{u}^0 - \nabla \cdot (\mathcal{K} \nabla p^0) + \mathrm{i}\omega \mathcal{H} p^0 = 0 \quad &\text{in } \Omega \\ \boldsymbol{u}^0 = \bar{\boldsymbol{u}} \quad \text{and} \quad (\mathcal{K} \nabla p^0 - \omega^2 \boldsymbol{\mathcal{G}}' \boldsymbol{u}^0) \cdot \boldsymbol{n} = 0 \quad &\text{on } \partial\Omega \end{aligned} \tag{13}$$

The following observations are worth noting from the last equations:

(i) Equations (13) are derived upon integrating by parts in the weak form of the limit problem (10). This yields the second boundary condition $(13)_3$ which expresses impermeability of the boundary and, thus, is coherent with $(2)_2$ imposed. Indeed, using the expressions of the homogenized coefficients $\mathcal{K}$ and $\boldsymbol{\mathcal{G}}'$ given in Section 4 (see (21), (22) and (19)), one may verify, that $\boldsymbol{w}^0(x) := \int_{Y_c} \boldsymbol{W}(x,\cdot) = \mathcal{K}\nabla p^0 - \omega^2 \boldsymbol{\mathcal{G}}' \boldsymbol{u}^0$ is the effective seepage velocity of the fluid. Hence, in fact, $(13)_3$ reads as $\boldsymbol{w}^0(x) \cdot \boldsymbol{n} = 0$.

(ii) In general, the symmetry of $\boldsymbol{\mathcal{G}}$ does not hold, *i.e.* $\mathcal{G}_{ij} \neq \mathcal{G}_{ji}$ (see $(11)_3$). As a consequence, the nonsymmetric gradient occurs in $(13)_2$, where $(\boldsymbol{\mathcal{G}})^{\mathrm{T}} : \nabla \boldsymbol{u}^0 = \mathcal{G}_{ij} \partial_j u^0_i$. This nonsymmetry indicates the presence of gyroscopic inertia effects due to the (relative) flow of fluid in the moving skeleton. Tensor $\boldsymbol{\mathcal{B}}$ is symmetric, however.

(iii) It can be shown that the poro-viscoelastic coefficients $\boldsymbol{\mathcal{D}}, \boldsymbol{\mathcal{B}}$, and $\mathcal{H}$ consist each of two parts: their poroelastic parts, $\bar{\boldsymbol{\mathcal{D}}}, \bar{\boldsymbol{\mathcal{B}}}$, and $\bar{\mathcal{H}}$ describe the static macroscopic response of the double-porous medium, or the quasistatic response, *i.e.* for frequencies $\omega \to 0$, whereas the other parts, *e.g.*, $\tilde{\boldsymbol{\mathcal{D}}}(\omega) = \boldsymbol{\mathcal{D}}(\omega) - \bar{\boldsymbol{\mathcal{D}}}$ (and similarly for the others coefficients), describe the memory effects induced by the flow in the dual porosity represented by the material properties in $Y_{\mathrm{m}}$. It is worth to remark that in the standard type of medium obeying the Biot model at the mesoscopic level, as treated in [30], *i.e.* without the strong heterogeneities, the frequency-dependent parts denoted above by $\tilde{(\,)}$ are not present.

To conclude this section, we compare the mesoscopic model governed by the set of three equations (1) with the upscaled model (13). While (1) involves the three fields $\boldsymbol{u}, \boldsymbol{w}, p$, the macroscopic limit model involves the mean displacements $\boldsymbol{u}^0$ and the mean pressure $p^0$. Although (13) can be rewritten in terms of $\boldsymbol{u}^0, p^0$, and $\boldsymbol{w}^0$ given by the generalized Darcy law discussed in (i) on the previous paragraph, it is straightforward to eliminate in (1) the seepage velocity $\boldsymbol{w}$, which yields (see (3), introducing the dynamic permeability $\boldsymbol{\kappa}(\omega)$):

$$
\begin{aligned}
-\omega^2 \boldsymbol{M}(\omega)\boldsymbol{u} - \nabla\cdot(\mathbb{D}\boldsymbol{e}(\boldsymbol{u})) - \mathbb{A}(\omega)p = 0\\
\mathrm{i}\omega\mathbb{A}^*(\omega)\boldsymbol{u} - \nabla\cdot(\boldsymbol{\kappa}(\omega)\nabla p) + \frac{\mathrm{i}\omega}{\mu}p = 0
\end{aligned}
\tag{14}
$$

where the operators $\mathbb{A}(\omega)$, $\mathbb{A}^*(\omega)$ and $\boldsymbol{M}(\omega)$ are defined by

$$
\begin{aligned}
-\mathbb{A}(\omega)p &= \nabla\cdot(\boldsymbol{\alpha}p) - \mathrm{i}\omega\rho^f\boldsymbol{\kappa}(\omega)\nabla p\\
\mathbb{A}^*(\omega)\boldsymbol{u} &= \boldsymbol{\alpha}:\nabla\boldsymbol{u} - \mathrm{i}\omega\rho^f\nabla\cdot(\boldsymbol{\kappa}(\omega)\boldsymbol{u})\\
\boldsymbol{M}(\omega) &= \bar{\rho}\boldsymbol{I} - \mathrm{i}\omega(\rho^{\mathrm{f}})^2\boldsymbol{\kappa}(\omega)
\end{aligned}
\tag{15}
$$

where $\boldsymbol{I}$ is the second-order identity tensor.

Note that the operator $\mathbb{A}^*$ adjoint to $\mathbb{A}$ is introduced for a more general situation corresponding to a locally periodic medium, so that all homogenized coefficients, thus, also $\boldsymbol{\alpha}$ and $\boldsymbol{\kappa}$, are differentiable functions of the macroscopic position in $\Omega$.

We shall comment on possible relationships between the structure of the mesoscopic model (14) and its upscaled representation (13) in the conclusion.

## 4. Local problems and homogenized coefficients

In this section, we introduce the local problems for computing the characteristic responses imposed in the representative cell $Y$. They are obtained from the system (7)–(9) upon substituting there vanishing macroscopic test functions, *i.e.* for $\boldsymbol{v}^0, q^0 = 0$. The homogenized coefficients are computed using these characteristic responses; the specific formulae will be given in Section 4.3. We recall the $Y$-periodicity of all the involved functions, which is indicated by the subscript #; thus $H^1_\#(Y)$ is the space $H^1(Y)$ involving the $Y$-periodic functions only. In particular, we employ the following space of "bubble functions" [31,32] (used for displacement field) and the space of seepage velocities

$$
\begin{aligned}
\mathbf{H}^1_{\#,0}(Y_{\mathrm{c}}) &= \{\boldsymbol{v}\in\mathbf{H}^1_\#(Y_{\mathrm{c}}) \mid \boldsymbol{v} = 0 \text{ on } \partial Y_{\mathrm{c}}\setminus\partial Y\}\\
\mathbf{H}_{0\#}(\mathrm{div}, Y_{\mathrm{c}}) &= \{\boldsymbol{w}\in\mathbf{H}_\#(\mathrm{div}, Y_{\mathrm{c}}) \mid \boldsymbol{w}\cdot\boldsymbol{n} = 0 \text{ on } \partial Y_{\mathrm{c}}\setminus\partial Y\ ,\ \nabla_y\cdot\boldsymbol{w} = 0\}
\end{aligned}
$$

An analogous space of scalar bubble functions, denoted by $H^1_{0,\#}(Y_{\mathrm{m}})$, is employed. To establish weak formulations of the local problems imposed in the matrix and in the channels of the mesostructure, we need the following two spaces:

$$
\begin{aligned}
\mathcal{A}_{\mathrm{m}} &= \mathbf{H}^1_\#(Y_{\mathrm{m}})\times H^1_{0,\#}(Y_{\mathrm{m}})\times\mathbf{L}^2_\#(Y_{\mathrm{m}})\\
\mathcal{A}_{\mathrm{c}} &= \mathbf{H}^1_{\#0}(Y_{\mathrm{c}})\times H^1_\#(Y_{\mathrm{c}})\times\mathbf{L}^2_\#(Y_{\mathrm{c}})
\end{aligned}
$$

### 4.1. Local problems in the matrix $Y_{\mathrm{m}}$

The first group of local responses is obtained by putting $\hat{\boldsymbol{v}}, Q^1, \boldsymbol{\Psi} = 0$ (in addition to $\boldsymbol{v}^0, q^0 = 0$ applied in (7) and (9)), which yields the following coupled system of equations governing the two-scale response in the matrix part of the mesostructure:

$$
\begin{aligned}
\int_{Y_{\mathrm{m}}}\mathbb{D}_{\mathrm{m}}(\boldsymbol{e}_x(\boldsymbol{u}^0)+\boldsymbol{e}_y(\boldsymbol{U}^1)):\boldsymbol{e}_y(\boldsymbol{V}^1) - \int_{Y_{\mathrm{m}}}\boldsymbol{\alpha}_{\mathrm{m}}:\boldsymbol{e}_y(\boldsymbol{V}^1)(p^0+\hat{p}) = 0\\
\int_{Y_{\mathrm{m}}}[\widehat{\boldsymbol{K}}_{\mathrm{m}}]^{-1}\hat{\boldsymbol{w}}\cdot\hat{\boldsymbol{\psi}} + \int_{Y_{\mathrm{m}}}\nabla_y\hat{p}\cdot\hat{\boldsymbol{\psi}} = 0\\
\mathrm{i}\omega\int_{Y_{\mathrm{m}}}\boldsymbol{\alpha}_{\mathrm{m}}:(\boldsymbol{e}_x(\boldsymbol{u}^0)+\boldsymbol{e}_y(\boldsymbol{U}^1))\hat{q} - \int_{Y_{\mathrm{m}}}\hat{\boldsymbol{w}}\cdot\nabla_y\hat{q} + \mathrm{i}\omega\int_{Y_{\mathrm{m}}}\frac{1}{\mu_{\mathrm{m}}}(p^0+\hat{p})\hat{q} = 0
\end{aligned}
\tag{16}
$$

which must hold for all $(\boldsymbol{V}^1, \hat{\boldsymbol{\psi}}, \hat{q})\in\mathcal{A}_{\mathrm{m}}$. The further step of the classical homogenization procedure consists in decoupling the scales, so that the characteristic responses can be distinguished. Due to the problem linearity, the following split can be defined:

$$
\begin{aligned}
\boldsymbol{U}^1 &= \mathrm{i}\omega\boldsymbol{\omega}^{kl}e^x_{kl}(\boldsymbol{u}^0) + \mathrm{i}\omega\boldsymbol{\omega}^P p^0\\
\hat{\boldsymbol{w}} &= \mathrm{i}\omega\hat{\boldsymbol{\chi}}^{kl}e^x_{kl}(\boldsymbol{u}^0) + \mathrm{i}\omega\hat{\boldsymbol{\chi}}^P p^0\\
\hat{p} &= \mathrm{i}\omega\hat{\pi}^{kl}e^x_{kl}(\boldsymbol{u}^0) + \mathrm{i}\omega\hat{\pi}^P p^0
\end{aligned}
\tag{17}
$$

We shall abbreviate the inner product in $Y_{\mathrm{m}}$ by $\langle\cdot,\cdot\rangle_{Y_{\mathrm{m}}}$ and use the following bilinear forms

$$a_{\rm m}(\boldsymbol{u},\,\boldsymbol{v}) = \int_{Y_{\rm m}} \mathbb{D}_{\rm m}\boldsymbol{e}_y(\boldsymbol{u}) : \boldsymbol{e}_y(\boldsymbol{v})\,, \qquad b_{\rm m}(p,\,\boldsymbol{v}) = \int_{Y_{\rm m}} \boldsymbol{\alpha}_{\rm m} : \boldsymbol{e}_y(\boldsymbol{v}) p$$

$$d_{\rm m}(p,\,q) = \int_{Y_{\rm m}} \frac{1}{\mu_{\rm m}} pq\,, \qquad c_{\rm m}(\boldsymbol{w},\,\boldsymbol{z}) = \int_{Y_{\rm m}} [\widehat{\boldsymbol{K}}_{\rm m}]^{-1}\boldsymbol{w}\cdot\boldsymbol{z}$$

Upon substituting (17) in (16), we obtain the two autonomous problems:

– Find $(\boldsymbol{\omega}^{kl}, \hat{\pi}^{kl}, \hat{\boldsymbol{\chi}}^{kl}) \in \mathcal{A}_{\rm m}$

$$a_{\rm m}\left(\boldsymbol{\omega}^{kl},\,\boldsymbol{v}\right) - b_{\rm m}\left(\hat{\pi}^{kl},\,\boldsymbol{v}\right) = -\frac{1}{{\rm i}\omega} a_{\rm m}\left(\boldsymbol{\Pi}^{kl},\,\boldsymbol{v}\right)$$

$$\left\langle \hat{\boldsymbol{z}},\,\nabla_y\hat{\pi}^{kl}\right\rangle_{Y_{\rm m}} + c_{\rm m}\left(\hat{\boldsymbol{\chi}}^{kl},\,\hat{\boldsymbol{z}}\right) = 0$$

$${\rm i}\omega b_{\rm m}\left(\hat{q},\,\boldsymbol{\omega}^{kl}\right) - \left\langle \hat{\boldsymbol{\chi}}^{kl},\,\nabla_y\hat{q}\right\rangle_{Y_{\rm m}} + {\rm i}\omega d_{\rm m}\left(\hat{\pi}^{kl},\,\hat{q}\right) = -b_{\rm m}\left(\hat{q},\,\boldsymbol{\Pi}^{kl}\right)$$

for all $(\boldsymbol{v}, \hat{q}, \hat{\boldsymbol{z}}) \in \mathcal{A}_{\rm m}$, where $\boldsymbol{\Pi}^{kl} = (\Pi_i^{kl})$ with $\Pi_i^{kl} = y_l\delta_{ik}$.

– Find $(\boldsymbol{\omega}^{P}, \hat{\pi}^{P}, \hat{\boldsymbol{\chi}}^{P}) \in \mathcal{A}_{\rm m}$

$$a_{\rm m}\left(\boldsymbol{\omega}^{P},\,\boldsymbol{v}\right) - b_{\rm m}\left(\hat{\pi}^{P},\,\boldsymbol{v}\right) = \frac{1}{{\rm i}\omega} b_{\rm m}(1,\,\boldsymbol{v})$$

$$\left\langle \hat{\boldsymbol{z}},\,\nabla_y\hat{\pi}^{P}\right\rangle_{Y_{\rm m}} + c_{\rm m}\left(\hat{\boldsymbol{\chi}}^{P},\,\hat{\boldsymbol{z}}\right) = 0$$

$${\rm i}\omega b_{\rm m}\left(\hat{q},\,\boldsymbol{\omega}^{P}\right) - \left\langle \hat{\boldsymbol{\chi}}^{P},\,\nabla_y\hat{q}\right\rangle_{Y_{\rm m}} + {\rm i}\omega d_{\rm m}\left(\hat{\pi}^{P},\,\hat{q}\right) = -d_{\rm m}\left(1,\,\hat{q}\right)$$

for all $(\boldsymbol{v}, \hat{q}, \hat{\boldsymbol{z}}) \in \mathcal{A}_{\rm m}$.

### 4.2. Local problems in the channel $Y_{\rm c}$

We pursue an analogous procedure reported in Section 4.1. The second group of the local problems is obtained upon substituting $\boldsymbol{V}^1, \hat{q}, \hat{\boldsymbol{\psi}} = 0$ (in addition to $\boldsymbol{v}^0, q^0 = 0$ applied in (7) and (9)). This leads to the local problem:

$$\begin{aligned}
&\int_{Y_{\rm c}} \widehat{\mathbb{D}}_{\rm c}\boldsymbol{e}_y(\hat{\boldsymbol{u}}) : \boldsymbol{e}_y(\hat{\boldsymbol{v}}) - \int_{Y_{\rm c}} \widehat{\boldsymbol{\alpha}}_{\rm c} : \boldsymbol{e}_y(\hat{\boldsymbol{v}}) p^0 + \int_{Y_{\rm c}} \left(-\omega^2\bar{\rho}_{\rm c}(\boldsymbol{u}^0 + \hat{\boldsymbol{u}}) + {\rm i}\omega\rho^{\rm f}\boldsymbol{W}\right)\cdot\hat{\boldsymbol{v}} = 0\\
&\int_{Y_{\rm c}} \left(-\omega^2\rho^{\rm f}(\boldsymbol{u}^0 + \hat{\boldsymbol{u}}) + {\rm i}\omega\boldsymbol{\rho}_{\rm c}\boldsymbol{W}\right)\cdot\boldsymbol{\psi} + \int_{Y_{\rm c}} [\boldsymbol{K}_{\rm c}]^{-1}\boldsymbol{W}\cdot\boldsymbol{\psi} + \int_{Y_{\rm c}} \tilde{\boldsymbol{w}}\cdot(\nabla_x p^0 + \nabla_y P^1) = 0\\
&\int_{Y_{\rm c}} \nabla_y q\cdot\boldsymbol{W} = 0
\end{aligned} \tag{18}$$

for all $(\hat{\boldsymbol{v}}, q, \boldsymbol{\psi}) \in \mathcal{A}_{\rm c}$.

We proceed in analogy with the previous paragraph and introduce the following splits:

$$\begin{aligned}
\hat{\boldsymbol{u}} &= {\rm i}\omega\hat{\boldsymbol{\omega}}^k\left(-\omega^2 u_k^0\right) + {\rm i}\omega\hat{\boldsymbol{\omega}}^P p^0 + {\rm i}\omega\hat{\boldsymbol{\omega}}^{\nabla P,k}\partial_k^x p^0\\
P^1 &= {\rm i}\omega\pi^k\left(-\omega^2 u_k^0\right) + {\rm i}\omega\pi^P p^0 + {\rm i}\omega\pi^{\nabla P,k}\partial_k^x p^0\\
\boldsymbol{W} &= {\rm i}\omega\boldsymbol{\chi}^k\left(-\omega^2 u_k^0\right) + {\rm i}\omega\boldsymbol{\chi}^P p^0 + {\rm i}\omega\boldsymbol{\chi}^{\nabla P,k}\partial_k^x p^0
\end{aligned} \tag{19}$$

The following bilinear forms are employed (we abbreviate the inner product in $Y_{\rm c}$ by $\langle\cdot,\,\cdot\rangle_{Y_{\rm c}}$)

$$a_{\rm c}(\boldsymbol{u},\,\boldsymbol{v}) = \int_{Y_{\rm c}} \widehat{\mathbb{D}}_{\rm c}\boldsymbol{e}_y(\boldsymbol{u}) : \boldsymbol{e}_y(\boldsymbol{v})\,, \qquad b_{\rm c}(p,\,\boldsymbol{v}) = \int_{Y_{\rm c}} \widehat{\boldsymbol{\alpha}}_{\rm c} : \boldsymbol{e}_y(\boldsymbol{v}) p$$

$$\varrho_{\rm c}(\boldsymbol{z},\,\boldsymbol{\psi}) = \int_{Y_{\rm c}} (\boldsymbol{\rho}_{\rm c}\boldsymbol{z})\cdot\boldsymbol{\psi}\,, \qquad c_{\rm c}(\boldsymbol{w},\,\boldsymbol{z}) = \int_{Y_{\rm c}} [\boldsymbol{K}_{\rm c}]^{-1}\boldsymbol{w}\cdot\boldsymbol{z}$$

The decomposition is substituted into the local problem (18), so that the following autonomous problems for the characteristic responses in domain $Y_{\rm c}$ are distinguished.

– Find $(\hat{\boldsymbol{\omega}}^k, \pi^k, \boldsymbol{\chi}^k) \in \mathcal{A}_{\rm c}$, such that

$$a_{\rm c}\left(\hat{\boldsymbol{\omega}}^k,\ \hat{\boldsymbol{v}}\right) - \omega^2\left\langle\bar{\rho}_{\rm c}\hat{\boldsymbol{\omega}}^k,\ \hat{\boldsymbol{v}}\right\rangle_{Y_{\rm c}} + {\rm i}\omega\left\langle\rho^{\rm f}\boldsymbol{\chi}^k,\ \hat{\boldsymbol{v}}\right\rangle_{Y_{\rm c}} = -\frac{1}{{\rm i}\omega}\left\langle\bar{\rho}_{\rm c}\boldsymbol{1}_k,\ \hat{\boldsymbol{v}}\right\rangle_{Y_{\rm c}}$$
$$-\omega^2\left\langle\rho^{\rm f}\hat{\boldsymbol{\omega}}^k,\ \boldsymbol{\psi}\right\rangle_{Y_{\rm c}} + {\rm i}\omega\varrho_{\rm c}\left(\boldsymbol{\chi}^k,\ \boldsymbol{\psi}\right) + c_{\rm c}\left(\boldsymbol{\chi}^k,\ \boldsymbol{\psi}\right) + \left\langle\nabla_y\pi^k,\ \boldsymbol{\psi}\right\rangle_{Y_{\rm c}} = -\frac{1}{{\rm i}\omega}\left\langle\rho^{\rm f}\boldsymbol{1}_k,\ \boldsymbol{\psi}\right\rangle_{Y_{\rm c}}$$
$$\left\langle\boldsymbol{\chi}^k,\ \nabla_y q\right\rangle_{Y_{\rm c}} = 0$$

for all $(\hat{\boldsymbol{v}}, q, \boldsymbol{\psi}) \in \mathcal{A}_{\rm c}$, where $\boldsymbol{1}_k = (\delta_{ik})$.

– Find $(\hat{\boldsymbol{\omega}}^P, \pi^P, \boldsymbol{\chi}^P) \in \mathcal{A}_{\rm c}$, such that

$$a_{\rm c}\left(\hat{\boldsymbol{\omega}}^P,\ \hat{\boldsymbol{v}}\right) - \omega^2\left\langle\bar{\rho}_{\rm c}\hat{\boldsymbol{\omega}}^P,\ \hat{\boldsymbol{v}}\right\rangle_{Y_{\rm c}} + {\rm i}\omega\left\langle\rho^{\rm f}\boldsymbol{\chi}^P,\ \hat{\boldsymbol{v}}\right\rangle_{Y_{\rm c}} = \frac{1}{{\rm i}\omega}b_{\rm c}\left(1,\ \hat{\boldsymbol{v}}\right)$$
$$-\omega^2\left\langle\rho^{\rm f}\hat{\boldsymbol{\omega}}^P,\ \boldsymbol{\psi}\right\rangle_{Y_{\rm c}} + {\rm i}\omega\varrho_{\rm c}\left(\boldsymbol{\chi}^P,\ \boldsymbol{\psi}\right) + c_{\rm c}\left(\boldsymbol{\chi}^P,\ \boldsymbol{\psi}\right) + \left\langle\nabla_y\pi^P,\ \boldsymbol{\psi}\right\rangle_{Y_{\rm c}} = 0$$
$$\left\langle\boldsymbol{\chi}^P,\ \nabla_y q\right\rangle_{Y_{\rm c}} = 0$$

for all $(\hat{\boldsymbol{v}}, q, \boldsymbol{\psi}) \in \mathcal{A}_{\rm c}$.

– Find $(\hat{\boldsymbol{\omega}}^{\nabla P,k}, \pi^{\nabla P,k}, \boldsymbol{\chi}^{\nabla P,k}) \in \mathcal{A}_{\rm c}$, such that

$$a_{\rm c}\left(\hat{\boldsymbol{\omega}}^{\nabla P,k},\ \hat{\boldsymbol{v}}\right) - \omega^2\left\langle\bar{\rho}_{\rm c}\hat{\boldsymbol{\omega}}^{\nabla P,k},\ \hat{\boldsymbol{v}}\right\rangle_{Y_{\rm c}} + {\rm i}\omega\left\langle\rho^{\rm f}\boldsymbol{\chi}^{\nabla P,k},\ \hat{\boldsymbol{v}}\right\rangle_{Y_{\rm c}} = 0$$
$$-\omega^2\left\langle\rho^{\rm f}\hat{\boldsymbol{\omega}}^{\nabla P,k},\ \boldsymbol{\psi}\right\rangle_{Y_{\rm c}} + {\rm i}\omega\varrho_{\rm c}\left(\boldsymbol{\chi}^{\nabla P,k},\ \boldsymbol{\psi}\right) + c_{\rm c}\left(\boldsymbol{\chi}^{\nabla P,k},\ \boldsymbol{\psi}\right) +$$
$$\left\langle\nabla_y\pi^{\nabla P,k},\ \boldsymbol{\psi}\right\rangle_{Y_{\rm c}} = -\frac{1}{{\rm i}\omega}\left\langle\boldsymbol{1}_k,\ \boldsymbol{\psi}\right\rangle_{Y_{\rm c}}$$
$$\left\langle\boldsymbol{\chi}^{\nabla P,k},\ \nabla_y q\right\rangle_{Y_{\rm c}} = 0$$

for all $(\hat{\boldsymbol{v}}, q, \boldsymbol{\psi}) \in \mathcal{A}_{\rm c}$.

Note that, alternatively, the autonomous problems for the local characteristic responses can be reduced using the obvious identity $\langle\nabla_y\pi,\ \boldsymbol{\chi}\rangle_{Y_{\rm c}} = -\langle\pi,\ \nabla\cdot\boldsymbol{\chi}\rangle_{Y_{\rm c}} = 0$ for any $(\pi, \boldsymbol{\chi}) \in H^1_{\#}(Y_{\rm c}) \times \mathbf{H}_{0\#}({\rm div}, Y_{\rm c})$. The same identity can be applied in (18); it follows easily (upon integrating by parts) that, for $\boldsymbol{W}(x,\cdot) \in \mathbf{H}_{0\#}({\rm div}, Y_{\rm c})$, the last equality in (18) vanishes and $\left\langle\nabla_y P^1,\ \tilde{\boldsymbol{w}}\right\rangle_{Y_{\rm c}} = 0$ as well. Therefore, there is no need to consider the decomposition (19) for $P^1$; consequently the local problems in $Y_{\rm c}$ attain the following generic structure.

Find $(\hat{\boldsymbol{\omega}}, \boldsymbol{\chi}) \in \mathbf{H}^1_{\#0}(Y_{\rm c}) \times \mathbf{H}_{0\#}({\rm div}, Y_{\rm c})$, such that

$$a_{\rm c}\left(\hat{\boldsymbol{\omega}},\ \hat{\boldsymbol{v}}\right) - \omega^2\left\langle\bar{\rho}_{\rm c}\hat{\boldsymbol{\omega}},\ \hat{\boldsymbol{v}}\right\rangle_{Y_{\rm c}} + {\rm i}\omega\left\langle\rho^{\rm f}\boldsymbol{\chi},\ \hat{\boldsymbol{v}}\right\rangle_{Y_{\rm c}} = -\frac{1}{{\rm i}\omega}f(\hat{\boldsymbol{v}})$$
$$-\omega^2\left\langle\rho^{\rm f}\hat{\boldsymbol{\omega}},\ \boldsymbol{\psi}\right\rangle_{Y_{\rm c}} + {\rm i}\omega\varrho_{\rm c}\left(\boldsymbol{\chi},\ \boldsymbol{\psi}\right) + c_{\rm c}\left(\boldsymbol{\chi},\ \boldsymbol{\psi}\right) = -\frac{1}{{\rm i}\omega}g(\boldsymbol{\psi})$$

for all $(\hat{\boldsymbol{v}}, \boldsymbol{\psi}) \in \mathbf{H}^1_{\#0}(Y_{\rm c}) \times \mathbf{H}_{0\#}({\rm div}, Y_{\rm c})$, where $f$ and $g$ designate a generic form of right hand side terms of the above problems.

Note that the two groups of the local problems in $Y_{\rm m}$ and $Y_{\rm c}$ are mutually decoupled.

### 4.3. Effective material coefficients of the homogenized medium

We now consider the two-scale limit problem (7)–(9) evaluated for vanishing "local" test functions, thus $\boldsymbol{V}^1, \hat{\boldsymbol{v}}, Q^1, \hat{q}, \boldsymbol{\psi}, \hat{\boldsymbol{\psi}} = 0$, and where we substitute the two-scale functions $\boldsymbol{U}^1, P^1, \hat{\boldsymbol{u}}, \hat{p}, \boldsymbol{W}$ decomposed using the characteristic responses (see (17) and (19)). Below we list formulae for all the homogenized coefficients involved in (10). They can be identified there upon collecting particular unknown and test functions; we give this reduced information, which explains the meaning of the associated homogenized coefficients.

– Effective viscoelasticity (combining $\boldsymbol{e}(\boldsymbol{u}^0)$ and $\boldsymbol{e}(\boldsymbol{v}^0)$ in (7))

$$\mathcal{D}_{ijkl}({\rm i}\omega) = {\rm i}\omega a_{\rm m}\left(\boldsymbol{\omega}^{kl} + \frac{1}{{\rm i}\omega}\boldsymbol{\Pi}^{kl},\ \boldsymbol{\omega}^{ij} + \frac{1}{{\rm i}\omega}\boldsymbol{\Pi}^{ij}\right) + c_{\rm m}\left(\hat{\boldsymbol{\chi}}^{ij},\ \hat{\boldsymbol{\chi}}^{kl}\right) + {\rm i}\omega d_{\rm m}\left(\hat{\pi}^{ij},\ \hat{\pi}^{kl}\right) \tag{20}$$

– Effective coefficients of the Biot stress coupling ($\mathcal{B}_{ij}$, and the "dynamic part" $\mathcal{G}_{ij}$ by combining $p^0$ and $\boldsymbol{e}_x(\boldsymbol{v}^0)$ in (7); $\mathcal{B}'_{ij}$ with the dynamic part $\mathcal{G}'_{ij}$ by combining $\boldsymbol{e}_x(\boldsymbol{u}^0)$ and $q^0$ in (9))

$$\begin{aligned}
\mathcal{B}_{ij} &= b_{\mathrm{m}}\left(1,\ \boldsymbol{\Pi}^{ij}\right) + \mathrm{i}\omega b_{\mathrm{m}}\left(\hat{\pi}^P,\ \boldsymbol{\Pi}^{ij}\right) - \mathrm{i}\omega a_m\left(\boldsymbol{\omega}^P,\ \boldsymbol{\Pi}^{ij}\right)\\
\mathcal{G}_{ij} &= \int_{Y_{\mathrm{c}}} \left(\mathrm{i}\omega\bar{\rho}_{\mathrm{c}}\hat{\omega}_i^{\nabla P,j} + \rho^{\mathrm{f}}\chi_i^{\nabla P,j}\right)\\
\mathcal{B}'_{ij} &= b_{\mathrm{m}}\left(1,\ \boldsymbol{\Pi}^{ij}\right) + \mathrm{i}\omega b_{\mathrm{m}}\left(1,\ \boldsymbol{\omega}^{ij}\right) + \mathrm{i}\omega d_{\mathrm{m}}\left(1,\ \hat{\pi}^{ij}\right)\\
\mathcal{G}'_{ij} &= -\mathrm{i}\omega\int_{Y_{\mathrm{c}}} \chi_i{}^j
\end{aligned} \tag{21}$$

– Effective permeability (by combining $\nabla p^0$ and $\nabla q^0$ in (9))

$$\mathcal{K}_{ij} = -\mathrm{i}\omega^{-1}\int_{Y_{\mathrm{c}}} \chi_i^{\nabla P,j} = \mathcal{K}_{ji} \tag{22}$$

– Effective coefficients of the Biot compressibility (by combining $p^0$ and $q^0$ in (9))

$$\mathcal{H} = \int_Y \mu^{-1} + \mathrm{i}\omega\left(\int_{Y_{\mathrm{m}}} \mu_{\mathrm{m}}^{-1}\hat{\pi}^P + b_{\mathrm{m}}\left(1,\ \boldsymbol{\omega}^P\right) + b_{\mathrm{c}}\left(1,\ \hat{\boldsymbol{\omega}}^P\right)\right) \tag{23}$$

– Effective mass (inertia) (by combining $-\omega^2\boldsymbol{u}^0$ and $\boldsymbol{v}^0$ in (7))

$$\mathcal{M}_{ij} = \int_Y \bar{\rho} + (\mathrm{i}\omega)^3\int_{Y_{\mathrm{c}}} \bar{\rho}_{\mathrm{c}}\hat{\omega}_i^j - \omega^2\int_{Y_{\mathrm{c}}} \rho^{\mathrm{f}}\chi_i{}^j = \mathcal{M}_{ji} \tag{24}$$

– Effective coefficients of the pressure-velocity coupling (combining $q^0$ and $\boldsymbol{u}^0$ in (7), further $p^0$ and $\boldsymbol{v}^0$ in (9)):

$$\begin{aligned}
\mathcal{C}_k &= -\omega^2\int_{Y_{\mathrm{c}}} \bar{\rho}_{\mathrm{c}}\hat{\omega}_k^P + \mathrm{i}\omega\int_{Y_{\mathrm{c}}} \rho^{\mathrm{f}}\hat{\chi}_k^P\\
\mathcal{C}'_k &= -\omega^2 b_{\mathrm{c}}\left(1,\ \hat{\boldsymbol{\omega}}^k\right)
\end{aligned} \tag{25}$$

### 4.4. Comments on the macroscopic model and the homogenized equation

A detailed analysis of the local problems in $Y_{\mathrm{m}}$ reveals that the characteristic responses $\boldsymbol{\omega}$ and $\pi$ can be decomposed into the constant and frequency-dependent parts, in particular

$$\begin{aligned}
\boldsymbol{\omega}^{kl}(y,\omega) &= \frac{1}{\mathrm{i}\omega}\bar{\boldsymbol{\omega}}^{kl}(y) + \tilde{\boldsymbol{\omega}}^{kl}(y,\omega)\,, \qquad \hat{\pi}^{kl}(y,\omega) = \frac{1}{\mathrm{i}\omega}\bar{\pi}^{kl}(y) + \tilde{\pi}^{kl}(y,\omega)\\
\boldsymbol{\omega}^{P}(y,\omega) &= \frac{1}{\mathrm{i}\omega}\bar{\boldsymbol{\omega}}^{P}(y) + \tilde{\boldsymbol{\omega}}^{P}(y,\omega)\,, \qquad \hat{\pi}^{P}(y,\omega) = \frac{1}{\mathrm{i}\omega}\bar{\pi}^{P}(y) + \tilde{\pi}^{P}(y,\omega)
\end{aligned} \tag{26}$$

For the other characteristic responses, $\hat{\boldsymbol{\chi}}^{kl}$ and $\hat{\boldsymbol{\chi}}^{P}$, we do not consider their constant parts. Since both the local autonomous problems imposed in $Y_{\mathrm{m}}$ are quite similar, we explain the decomposition for the one related to the strains $e^x_{kl}(\boldsymbol{u}^0)$. Substitution of $\boldsymbol{\omega}^{kl}$ and $\hat{\pi}^{kl}$ using (26) yields the following two subproblems, which can be resolved subsequently.

– Find $(\bar{\boldsymbol{\omega}}^{kl}, \bar{\pi}^{kl}) \in \mathcal{A}_{\mathrm{m}}$, such that

$$\begin{aligned}
a_{\mathrm{m}}\left(\bar{\boldsymbol{\omega}}^{kl},\ \boldsymbol{v}\right) - b_{\mathrm{m}}\left(\bar{\pi}^{kl},\ \boldsymbol{v}\right) &= -a_{\mathrm{m}}\left(\boldsymbol{\Pi}^{kl},\ \boldsymbol{v}\right)\\
b_{\mathrm{m}}\left(\hat{q},\ \bar{\boldsymbol{\omega}}^{kl}\right) + d_{\mathrm{m}}\left(\bar{\pi}^{kl},\ \hat{q}\right) &= -b_{\mathrm{m}}\left(\hat{q},\ \boldsymbol{\Pi}^{kl}\right)
\end{aligned}$$

for all $(\boldsymbol{v}, \hat{q}) \in \mathcal{A}_{\mathrm{m}}$.

– Find $(\tilde{\boldsymbol{\omega}}^{kl}, \tilde{\pi}^{kl}, \tilde{\boldsymbol{\chi}}^{kl}) \in \mathcal{A}_{\mathrm{m}}$, such that

$$
\begin{aligned}
a_{\mathrm{m}}\left(\tilde{\boldsymbol{\omega}}^{kl},\, \boldsymbol{v}\right) - b_{\mathrm{m}}\left(\tilde{\pi}^{kl},\, \boldsymbol{v}\right) &= 0\\
\left\langle \hat{\boldsymbol{z}},\, \nabla_y \tilde{\pi}^{kl}\right\rangle_{Y_{\mathrm{m}}} + c_{\mathrm{m}}\left(\hat{\boldsymbol{\chi}}^{kl},\, \hat{\boldsymbol{z}}\right) &= -\frac{1}{\mathrm{i}\omega}\left\langle \hat{\boldsymbol{z}},\, \nabla_y \bar{\pi}^{kl}\right\rangle_{Y_{\mathrm{m}}}\\
\mathrm{i}\omega b_{\mathrm{m}}\left(\hat{q},\, \tilde{\boldsymbol{\omega}}^{kl}\right) - \left\langle \hat{\boldsymbol{\chi}}^{kl},\, \nabla_y \hat{q}\right\rangle_{Y_{\mathrm{m}}} + \mathrm{i}\omega d_{\mathrm{m}}\left(\tilde{\pi}^{kl},\, \hat{q}\right) &= 0
\end{aligned}
$$

for all $(\boldsymbol{v}, \hat{q}, \hat{\boldsymbol{z}}) \in \mathcal{A}_{\mathrm{m}}$.

We can now rewrite the effective coefficients of the poroviscoelastic $\mathcal{D}$, $\mathcal{B}$, and $\mathcal{H}$ by decomposing them into the poroelastic parts and the dissipative (frequency-dependent) parts, as announced at the end of the Section 3.2. The following expressions hold

$$
\begin{aligned}
\mathrm{i}\omega\bar{\mathcal{D}}_{ijkl} &= a_{\mathrm{m}}\left(\bar{\boldsymbol{\omega}}^{kl} + \boldsymbol{\Pi}^{kl},\, \bar{\boldsymbol{\omega}}^{ij} + \boldsymbol{\Pi}^{ij}\right) + d_{\mathrm{m}}\left(\bar{\pi}^{ij},\, \bar{\pi}^{kl}\right)\\
\tilde{\mathcal{D}}_{ijkl}(\mathrm{i}\omega) &= -\mathrm{i}\omega a_{\mathrm{m}}\left(\tilde{\boldsymbol{\omega}}^{kl},\, \tilde{\boldsymbol{\omega}}^{ij}\right) - c_{\mathrm{m}}\left(\hat{\boldsymbol{\chi}}^{ij},\, \hat{\boldsymbol{\chi}}^{kl}\right) - \mathrm{i}\omega d_{\mathrm{m}}\left(\tilde{\pi}^{ij},\, \tilde{\pi}^{kl}\right)
\end{aligned}
\tag{27}
$$

The Biot coupling coefficients and the compressibility are decomposed by analogy:

$$
\begin{aligned}
\bar{\mathcal{B}}_{ij} &= b_{\mathrm{m}}\left(1 + \hat{\pi}^{P},\, \boldsymbol{\Pi}^{ij}\right) - a_{\mathrm{m}}\left(\bar{\boldsymbol{\omega}}^{P},\, \boldsymbol{\Pi}^{ij}\right)\\
\tilde{\mathcal{B}}_{ij}(\mathrm{i}\omega) &= \mathrm{i}\omega\left[b_{\mathrm{m}}\left(\tilde{\pi}^{P},\, \boldsymbol{\Pi}^{ij}\right) - a_{\mathrm{m}}\left(\tilde{\boldsymbol{\omega}}^{P},\, \boldsymbol{\Pi}^{ij}\right)\right]\\
\bar{\mathcal{H}} &= \int_Y \mu^{-1} + \int_{Y_{\mathrm{m}}} \mu_{\mathrm{m}}^{-1}\bar{\pi}^{P} + b_{\mathrm{m}}\left(1,\, \bar{\boldsymbol{\omega}}^{P}\right)\\
\tilde{\mathcal{H}}(\mathrm{i}\omega) &= \mathrm{i}\omega\left(\int_{Y_{\mathrm{m}}} \mu_{\mathrm{m}}^{-1}\tilde{\pi}^{P} + b_{\mathrm{m}}\left(1,\, \tilde{\boldsymbol{\omega}}^{P}\right) + b_{\mathrm{c}}\left(1,\, \hat{\boldsymbol{\omega}}^{P}\right)\right)
\end{aligned}
\tag{28}
$$

## 5. Concluding remarks

This paper presents an extension of the model describing the acoustic waves in the double porosity medium featured by the rigid skeleton [10,21]. In these works, we studied how the macroscopic description is influenced by the static permeability contrast between the micro- and meso-pores. As the new ingredients of the present study, the double porosity medium is constituted by the elastic deformable matrix which is characterized by a "high contrast" between the two subdomains in addition to a "high contrast" in the permeabilities and a moderated contrast in the Biot coupling coefficients.

The dispersion analysis can be done in a much similar way, as it has been done, *e.g.*, in [30]. Some preliminary numerical results on the phase velocity and the attenuation show the presence of two pressure waves and a significant dispersion, see [33]. A complete paper focusing on this aspect is under preparation.

It is worth noting that, if the double-porosity medium is drained (empty pores), the model reduces to an elastic composite with large contrasts in the elasticity coefficients – the band gaps have been studied using the homogenization approach in works [24,27] and other related papers, see [25]. If the fluid resides in pores, the presence of band gaps is not proved for the moment; however, as pointed out above, a strong dispersion occurs. Depending on the fluid viscosity, band gaps may appear.

The microflow in the double porosity is responsible for the fading memory effects via the macroscopic poroviscoelastic constitutive law. We have shown that all the effective material properties depend on the angular frequency $\omega$ in the frequency domain. This leads to convolution integrals in time, when transformed in the time domain. Thus, stresses are functions not only of the instantaneous deformation, but also depend on the whole past history of deformation. However, time-independent parts of the convolution kernels can be identified (*e.g.*, elasticity and viscosity properties are both contained in $\mathcal{D}$).

## Acknowledgements

E. Rohan is grateful to the "Centre national de la recherche scientifique" and "Université Paris-Est Créteil" for financial support received during the course of this research. This work has also been supported in part by project GACR P101/12/2315 of the Czech Scientific Foundation. V.-H. Nguyen and S. Naili have been supported by the Université Paris-Est and CNRS through the PEPS program (15R03051AMETCARMAT).

## References


[1] G.I. Barenblatt, I.P. Zheltov, I.N. Kochina, Basic concepts in the theory of seepage of homogeneous liquids in fissured rocks, PMM – Sov. Appl. Math. Mech. 24 (5) (1960) 852–864.
[2] R.K. Wilson, E.C. Aifantis, On the theory of consolidation with double porosity, Int. J. Eng. Sci. 20 (3) (1982) 1009–1035.
[3] J.-L. Auriault, C. Boutin, Deformable porous media with double porosity. Quasi statics. I. Coupling effects, Transp. Porous Media 7 (1) (1982) 63–82.
[4] J.-L. Auriault, C. Boutin, Deformable porous media with double porosity. Quasi statics. II. Memory effects, Transp. Porous Media 10 (2) (1993) 153–169.
[5] J.-L. Auriault, C. Boutin, Deformable porous media with double porosity III. Acoustics, Transp. Porous Media 14 (1994) 143–162.
[6] J.B. Berryman, H.F. Wang, Elastic wave propagation and attenuation in a double-porosity dual-permeability medium, Int. J. Rock Mech. Min. Sci. 37 (2000) 63–78.
[7] S.R. Pride, J.G. Berryman, Linear dynamics of double-porosity dual-permeability materials. I. Governing equations and acoustic attenuation, Phys. Rev. E 68 (2003) 036603.
[8] S.R. Pride, J.G. Berryman, Linear dynamics of double-porosity dual-permeability materials. II. Fluid transport equations, Phys. Rev. E 68 (2003) 036604.
[9] J. Ba, J.M. Carcione, J.X. Nie, Biot–Rayleigh theory of wave propagation in double-porosity media, J. Geophys. Res. 116 (2011) B06202, http://dx.doi.org/10.1029/2010JB008185.
[10] E. Rohan, Homogenization of acoustic waves in strongly heterogeneous porous structures, Wave Motion 50 (2013) 1073–1089.
[11] A. Bensoussan, J.-L. Lions, G. Papanicolaou, Asymptotic Methods in Periodic Media, North-Holland, 1978.
[12] É. Sanchez-Palencia, Non-homogeneous Media and Vibration Theory, Lecture Notes in Physics, vol. 127, Springer, Berlin, 1980.
[13] D. Cioranescu, P. Donato, An Introduction to Homogenization, Oxford Lecture Series in Mathematics and Its Applications, vol. 17, Oxford University Press, New York, 1999.
[14] G. Allaire, Homogenization and two-scale convergence, SIAM J. Math. Anal. 23 (1992) 1482–1518.
[15] D. Cioranescu, A. Damlamian, G. Griso, The periodic unfolding method in homogenization, SIAM J. Math. Anal. 40 (4) (2008) 1585–1620.
[16] H. Brézis, Functional Analysis, Sobolev Spaces and Partial Differential Equations, Springer, New York, 2010.
[17] M.A. Biot, Theory of propagation of elastic waves in a fluid-saturated porous solid. I. Low-frequency range, J. Acoust. Soc. Amer. 28 (2) (1956) 168–178.
[18] M.A. Biot, Theory of propagation of elastic waves in a fluid-saturated porous solid. II. Higher-frequency range, J. Acoust. Soc. Amer. 28 (2) (1956) 179–191.
[19] J.-L. Auriault, L. Borne, R. Chambon, Dynamics of porous saturated media, checking of the generalized law of Darcy, J. Acoust. Soc. Amer. 77 (5) (1985) 1641–1650.
[20] A.N. Norris, On the viscodynamic operator in Biot's equations of poroelasticity, J. Wave-Mater. Int. 1 (1986) 365–380.
[21] V.-H. Nguyen, E. Rohan, S. Naili, Multiscale simulation of acoustic waves in homogenized strongly heterogeneous porous media, Int. J. Eng. Sci. 101 (2016) 92–109.
[22] T. Arbogast, J. Douglas, U. Hornung, Derivation of the double porosity model of single phase flow via homogenization theory, SIAM J. Math. Anal. 21 (1990) 823–836.
[23] E. Rohan, S. Naili, R. Cimrman, T. Lemaire, Multiscale modeling of a fluid saturated medium with double porosity: Relevance to the compact bone, J. Mech. Phys. Solids 60 (2012) 857–881.
[24] A. Avila, G. Griso, B. Miara, E. Rohan, Multiscale modeling of elastic waves: theoretical justification and numerical simulation of band gaps, Multiscale Model. Simul. 7 (2008) 1–21.
[25] E. Rohan, B. Miara, F. Seifrt, Numerical simulation of acoustic band gaps in homogenized elastic composites, Int. J. Eng. Sci. 47 (2009) 573–594.
[26] E. Rohan, B. Miara, Band gaps and vibration of strongly heterogeneous Reissner–Mindlin elastic plates, C. R. Acad. Sci. Paris, Ser. I 349 (2011) 777–781.
[27] V.P. Smyshlyaev, Propagation and localization of elastic waves in highly anisotropic periodic composites via two-scale homogenization, Mech. Mater. 41 (2009) 434–447.
[28] D. Cioranescu, A. Damlamian, G. Griso, Periodic unfolding and homogenization, C. R. Acad. Sci. Paris, Ser. I 335 (2002) 99–104.
[29] E. Rohan, S. Naili, T. Lemaire, Double porosity in fluid-saturated elastic media: deriving effective parameters by hierarchical homogenization of static problem, Contin. Mech. Thermodyn. (2016), http://dx.doi.org/10.1007/s00161-015-0475-9, in press.
[30] A. Mielke, E. Rohan, Homogenization of elastic waves in fluid-saturated porous media using the Biot model, Math. Models Methods Appl. Sci. 23 (2013) 873–916.
[31] M. Crouzeix, P.-A. Raviart, Conforming and nonconforming finite element methods for solving the stationary Stokes equations, RAIRO. Anal. Numér. 3 (1973) 33–75.
[32] D. Arnold, F. Brezzi, M. Fortin, A stable finite element for the Stokes equations, Calcolo 21 (4) (1984) 337–344.
[33] E. Rohan, V.-H. Nguyen, S. Naili, Wave propagation in strongly heterogeneous fluid saturated porous medium: asymptotic analysis and computational issues, in: Proc. 6th Int. Conf. on Structural Engineering, Mechanics and Computation, SEMC 2016, Taylor & Francis/Balkema, 2016.